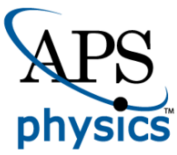

Reflection and Refraction of Flexural Waves at Geometric Boundaries

Arthur A. Evans and Alex J. Levine

Phys. Rev. Lett. **111**, 038101 — Published 16 July 2013

DOI: 10.1103/PhysRevLett.111.038101

Reflection and Refraction of Flexural Waves at Geometric Boundaries

Arthur A. Evans[1] and Alex J. Levine[1,2,3]
[1] *Department of Chemistry & Biochemistry, UCLA, Los Angeles CA 90095-1596, USA*
[2] *Department of Physics & Astronomy, UCLA, Los Angeles CA 90095-1596, USA and*
[3] *Department of Biomathematics, UCLA, Los Angeles CA 90095-1596, USA.*

We present a theory of flexural wave propagation on elastic shells having nontrivial geometry, and develop an analogy to geometric optics. The transport of momentum within the shell itself is anisotropic due to the curvature, and as such complex classical effects such as birefringence are generically found. We determine the equations of reflection and refraction of such waves at boundaries between different local geometries, showing that waves are totally internally reflected, especially at boundaries between regions of positive and negative Gaussian curvature. We verify these effects using finite element simulations and discuss the ramifications of these effects for the statistical mechanics of thin curved materials.

PACS numbers:

Curved shells appear in nature over a vast range of length scales from carbon nanotubes [1] to continental plates [2]. Understanding their mechanics and, in some cases, equilibrium fluctuations plays a key role in a variety of systems of interest in biological physics and material science such as viral capsids [3, 4], cellular membranes [5–7], plant morphogenesis [8], and self-assembled origami [9–11]. In spite of the large range of length scales and material properties, the mechanics of these shells are unified by the constraints imposed by the coupling of elasticity and geometry in materials whose lateral extent is much larger than their thickness.

This geometric property leads to a dramatic separation of the energy scales associated with bending and stretching. Generically, thin sheets and filaments are significantly softer to bending, allowing a unified treatment of wrinkling, crumpling, and a host of other morphological transitions under external forces or confinement [12–18]. Shells having a more complex geometry in their unstrained state, however, develop an inherent resistance to bending from the geometric coupling of the soft bending mode to the stiffer stretching one [19, 20], as a consequence of Gauss's *Theorema Egregium*, which relates changes in Gaussian curvature to stretching of the surface. Recently, an analysis of curved shell indentation by Vaziri and Mahadevan [21] of the response to static locally imposed forces has shown that the linear response of the deformation field depends qualitatively on the sign of the Gaussian curvature.

Motivated by this analysis, we examine in this Letter the propagation of flexural waves in shallow shells of constant curvature. We show that there is a useful analogy between this problem and the more familiar analysis of the propagation of light with the local curvature playing the role of the index of refraction. We derive an analog of Snell's law for refraction between two interfaces with differing optical properties; in our case, the material is identical across the interface, but only the local geometry changes. We find that curved shells are generically birefringent and may exhibit total internal reflection. Additionally, waves within regions of negative curvature propagate primarily along certain directions, and interfaces separating positive and negative Gaussian curvature regions lead generically to a range of incident angles that exhibit total internal reflection. The combination of these two effects indicates that curved elastic manifolds may act as barriers causally disconnecting regions of differing Gaussian curvature, leading to anomalously slow phonon equilibration, with potential implications for the statistical mechanics of such surfaces.

Even with a linear constitutive relation for the material's elasticity, the equations governing elasticity of thin surfaces are nonlinear due to geometry. For certain cases, however, they may be linearized and useful expressions coaxed from the more general ones. The energy functional that describes a thin, elastic shell is given by $\mathcal{F} = \int_S (N^{\alpha\beta}E_{\alpha\beta} + M^{\alpha\beta}K_{\alpha\beta})$, where $E_{\alpha\beta}$ and $K_{\alpha\beta}$ are the deformation tensors associated with strain and bending of a surface, respectively. A linearly elastic material allows us to write the local stress tensor as $N^{\alpha\beta} = Yh[(1-\nu)E_{\alpha\beta} + \nu E^{\gamma}_{\gamma}]$ and the bending moment tensor as $M^{\alpha\beta} = \kappa[(1-\nu)K^{\alpha\beta} + \nu K^{\gamma}_{\gamma}]$; these linear functionals of the curvature and deformation tensors of the surface introduce the Young's Y and bending κ moduli, the shell's thickness h and Poisson ratio ν. The details are standard and can be found in Refs. [22, 23].

The Euler-Lagrange equations that result from this expression are nonlinear both in geometry and deformation. In only a few situations are there known analytic solutions that take into account the nonlinearities of geometric origin [24, 25]. Conversely, by considering a flat shell but retaining the nonlinearities in the deformation state, one arrives at the Föppl-von Kármán equations, which are notoriously difficult to solve [26]. We will consider the intermediate asymptotic limit of the Donnell-Mushtari-Vlasov (DMV) equations [21, 22], where nonlinearities in the deformation field are neglected but stresses introduced by leading order curvature terms are retained.

In this case the deformation tensors may be written in terms of the in-plane displacements v_α, the normal displacement ζ, and the curvature tensor of the undeformed shell $d_{\alpha\beta}$ as

$$K_{\alpha\beta} \approx D_\alpha D_\beta \zeta \tag{1}$$

$$E_{\alpha\beta} \approx \frac{1}{2}(D_\alpha v_\beta + D_\beta v_\alpha) - d_{\alpha\beta}\zeta, \tag{2}$$

with D_α the covariant derivative on the surface. These approximations neglect terms higher order than $O(d_{\alpha\beta})$ in the stress. This results in neglecting terms of the form $d_{\alpha\gamma}d^\gamma_\beta M^{\alpha\beta}$ and $D_\alpha(d^\beta_\gamma M^{\gamma\alpha})$ in the force balance, substantially simplifying the analysis. In the absence of $d_{\alpha\beta}$ these deformation tensors reduce to the flat case and the equations of plate elasticity are recovered. In anticipation of examining a "shallow" shell, we assume that the spatial extent of the deformations are small compared to the shell's radii of curvature, so we may replace covariant derivatives by partial derivatives: $D_\alpha \to \partial_\alpha$. In the same limit we may simplify the in-plane stresses by introducing the Airy stress function χ, defined by $N^{\alpha\beta} = \epsilon^{\alpha\eta}\epsilon^{\beta\xi}\partial_\eta\partial_\xi\chi$ ($\epsilon^{\alpha\beta}$ is the 2D alternating tensor). We are immediately led to the following equations of undulatory dynamics (in vacuum) and compatibility of the surface [22]:

$$\kappa\nabla^4\zeta - \mathcal{L}[\chi] = -\rho h\frac{\partial^2\zeta}{\partial t^2} \tag{3}$$

$$\frac{1}{Yh}\nabla^4\chi + \mathcal{L}[\zeta] = 0, \tag{4}$$

where ρ is the shell's mass density. The linear operator $\mathcal{L} = \epsilon^{\alpha\eta}\epsilon^{\beta\xi}d_{\alpha\beta}\partial_\eta\partial_\xi$ is a measure of the incompatibility of the surface with the flat space solution [27] and couples bending and stretching through the local curvature.

In analogy to the standard development of Snell's law in which one considers the propagation of light across an interface separating two regions with differing but spatially uniform dielectric constants, we consider flexural waves propagating from one region of constant curvature to another – see Fig.1a. A continuously varying local geometry may later be accounted for by a succession of such interfaces between regions of constant curvature. A flexural wave propagates through one region, with a given (possibly anisotropic) dispersion relation, impinges upon a region of differing geometry and must conserve momentum at the interface due to translational invariance; hence, momentum conservation requires refraction [28]. Unlike in classical optics where any two dielectric constants may, in principle, be in contact, the continuity of the surface and its local slopes forces the principal curvature along the interface to remain constant. Consequently, there are only four possible combinations of curvature mismatch allowed at an interface – see Fig. 1b. In all cases we choose a coordinate system aligned with the principal axes of curvature; it will be useful to further parameterize their geometry by defining $\beta = R_x/R_y$ to be the ratio of these principal curvatures.

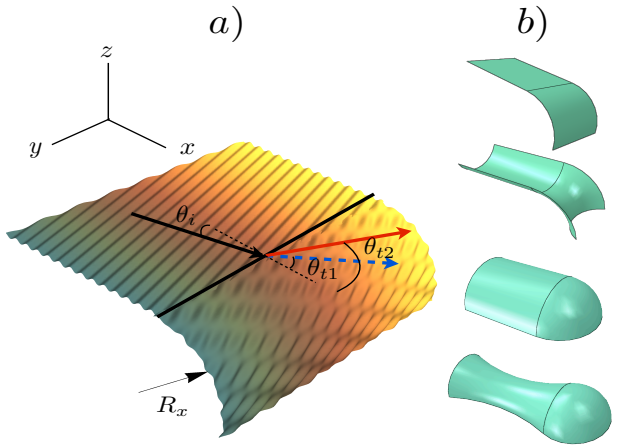

FIG. 1: (Color online) (a) Schematic of flexural waves refracting upon passage from one region of curvature to another, separated by the black line. Two refracted waves are produced in the birefringent (cylindrical) region on the right. (b) Prototypical interface types for traveling flexural waves on curved surfaces. Along the interface, kinematic constraints require the curvature to be continuous, leaving only a small number of possible choices.

To examine the dispersion relation for traveling plane waves in regions of constant geometry, we look for solutions of Eqs. 3,4 of the form $\zeta(\boldsymbol{x},t) = e^{i\boldsymbol{q}\cdot\boldsymbol{x}-i\omega t}\hat{\zeta}(\boldsymbol{q},\omega)$, $\chi(\boldsymbol{x},t) = e^{i\boldsymbol{q}\cdot\boldsymbol{x}-i\omega t}\hat{\chi}(\boldsymbol{q},\omega)$ obtaining a dispersion relation $\omega(\boldsymbol{q})$ as the solution to [29, 30]

$$\rho h\omega^2 = \kappa q^4 + \frac{Yh}{q^4}\mathcal{L}_q^2 \tag{5}$$

$$\mathcal{L}_q = \frac{q_y^2}{R_x} + \frac{q_x^2}{R_y}, \tag{6}$$

From this solution we determine the group velocity $\mathbf{v}_g = \partial\omega/\partial\mathbf{q}$ of flexural waves to be

$$\omega(\boldsymbol{q})\frac{\partial\omega}{\partial\mathbf{q}} = 2q^3\hat{\mathbf{q}} + \frac{(1-\beta)\sin 2\theta}{q}(\sin^2\theta + \beta\cos^2\theta)\hat{\mathbf{q}}^\perp, \tag{7}$$

where θ is the angle between $\boldsymbol{q}$ and the x-axis, and we have non-dimensionalized times and lengths by $\omega \to \omega/\omega_R$ and $q \to q\ell$ where $\omega_R^2 = Y/(R_x^2\rho)$ is the radial "ringing frequency" of a cylinder of radius R_x, and $\ell^4 = \kappa R_x^2/Yh$. For $q\ell \ll 1$ the shell can be considered in the "membrane" limit, where bending terms can be completely neglected. For $q\ell \gg 1$ the shell is essentially flat. Our analysis focuses on $q\ell \sim 1$. The first term in Eq. (7) reproduces the usual flexural wave dispersion relation for thin plates $\rho h\omega^2 = \kappa q^4$, while the second term carries momentum perpendicular to the wave vector and depends on curvature. The magnitude of the group velocity is also anisotropic as shown in Fig. 2 for saddle, ellipsoidal, and cylindrical surfaces.

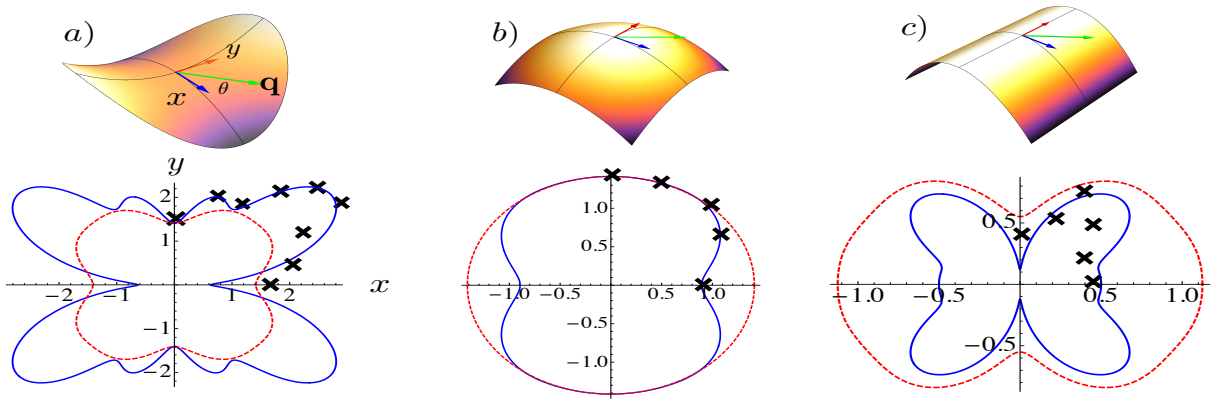

FIG. 2: (Color online) Examples of anisotropic flexural wave group velocities for different values of β. Figures show group velocities on a polar plot, with θ measured from the positive $x-$axis. Black symbols show group velocity measurements from finite element simulations – see supplemental information – to be compared to the (solid, blue) predictions of the linearized theory. a) For saddles, $\beta < 0$ the velocity has at least four lobes of maximum speed (compare to the static deformation characteristics in Ref. [21]) as seen for $\beta = -1, -3$ solid (blue) and dashed (red) lines respectively, with $q = 1$. b) Group velocities at $q = 1$ for ellipsoidal surfaces for $\beta = 1$ (solid, blue), a sphere, and $\beta = 2$ (dashed, red) show smaller variations with direction. c) Cylinders are more pathological because $\beta = 0$ and the Gaussian curvature is zero. As a result, the anisotropy depends solely on the wavenumber: $q = 0.5, 0.75$ solid (blue) and dashed (red) respectively. This pathology is seen most clearly in the magnitude of disagreement between the linearized theory and the finite element simulations; see supplemental information for more details.

For a generic anisotropic surface, a flexural ray will bend with respect to the principal axes. In order to address this, consider the anisotropic term in Eq. 7: $(1-\beta)\sin(2\theta)(\sin^2\theta + \beta\cos^2\theta)$. Except for a sphere ($\beta = 1$), this term is generally nonvanishing so that the group and phase velocities are not collinear, unless the waves propagate along the principal curvature directions $\theta^* = 0, \pi/2$. When not along one of these special directions where they do not bend, rays bend towards the direction of smallest curvature for $\beta > 0$ [31]. For $\beta < 0$, there is a new special direction $\theta^* = \tan^{-1}\sqrt{-\beta}$: if $\theta < \theta^*$ the rays bend towards the x-axis, otherwise they bend towards the y-axis. These results can be understood in terms of Fermat's principle [29, 31, 32].

We now turn to the refraction and reflection at the boundary between two different geometries. A ray with wave vector $\mathbf{q}$ making an angle of θ_i with respect to the x axis is injected into a region with principal curvature ratio β_i and encounters a boundary along the y-axis (see figure 1) with a different geometry, parametrized by β_t, and wave number $\mathbf{k}$. Matching the undeformed surface at the boundary requires R_y to be continuous through the interface, resulting in four allowed configurations – see Fig. 1b. We calculate the transmitted angle θ_t with respect to the boundary normal – see Fig. 1 – in terms of the incident angle θ_i by imposing conservation of the momentum tangent to the interface, i.e. $|\mathbf{q}|\sin\theta_i = |\mathbf{k}|\sin\theta_t$, resulting in the Snell's law analog

$$\left[\omega^2 - \mathcal{A}(\beta_i,\theta_i)\right]^{1/4}\sin\theta_i = \left[\omega^2 - \mathcal{A}(\beta_t,\theta_t)\right]^{1/4}\sin\theta_t, \tag{8}$$

where $\mathcal{A}(\beta,\theta) = (\beta\cos^2\theta + \sin^2\theta)^2$ contains the geometric information. The simplest form of these results are for plate, cylinder, sphere, and saddle where $\mathcal{A} = 0, \sin^4\theta, 1,$ and $\cos^2(2\theta)$ respectively.

Several representative curves of θ_t as a function of θ_i are shown in Fig. 3a (for simplicity we use only $\beta = 0, \pm 1$). The dashed and solid curves show the transmitted ray angles – two solutions are possible in birefringent cases. There are no solutions in the grey regions indicating total internal reflection (TIR). We do not show results for the sphere/cylinder interface, since we wish to highlight the effects of anisotropy on birefrigence and TIR; these effects are far more pronounced in the other prototypical interfaces. Consider as an example the plate/cylinder interface (see supplement for numerical tests of this case), where the incident region has $\mathcal{A} = 0$, while the cylindrical region has $\mathcal{A}(0,\theta_t) = \sin^4\theta_t$. Because the cylindrical region has an anisotropic dispersion relation, the phase velocity can be multivalued, and, in order to conserve momentum, it is possible that two rays are transmitted. This birefringence occurs in anisotropic dielectric media as well, and results from the multi-valuedness of the phase velocity in the medium [33]. Interfaces that include regions of negative Gaussian curvature include bands of TIR, as opposed to a critical angle above which all the incident rays are reflected. The solutions of Eq. 8 depend on both frequency and incident angle. Scanning over the input parameters, we arrive at the plots shown in Fig. 3b in which regions of single transmitted ray propagation (S), dual ray propagation (B), and total internal reflection (T) are shown. For large ω the curvature effects disappear, as the interface becomes transparent to sufficiently short wavelengths, except at

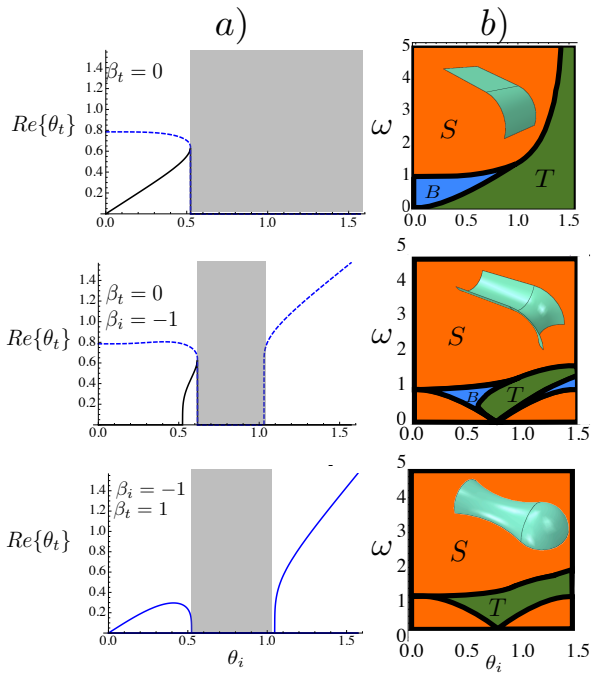

FIG. 3: (Color online) Transmitted angle as a function of the incident angle, for $\omega = 0.5$. a) Representative curves for $\mathcal{R}e\{\theta_t\}$ as a function of θ_i. Gray regions represent areas where $\mathcal{I}m\{\theta_t\} \neq 0$, indicating total internal reflection. b) Single mode transmission (S), birefringence (B), and total internal reflection (T) at different frequencies for different geometries (displayed as insets).

grazing incidence. It is of particular interest that in saddle regions most of the energy propagates at particular angles that depend on β; this point taken in tandem with the Snell's law results indicates that for the right value of β and ω flexural waves will be trapped within the negative Gauss curvature regions.

To test these analytic results, we performed finite element simulations using ABAQUS (Dassault Systemés) on a closed shell having boundaries between regions of constant geometry; see supplemental information for simulation details. The most dramatic results are obtained at boundaries between positive and negative Gaussian curvature. Consequently, we examine the "peanut" shell in Fig. 4 formed from a catenoid-like region (negative Gauss curvature) with $\beta \approx -0.5$ bounded at the top and bottom by spherical caps $\beta = 1$. The boundaries are shown by (black) dashed lines. At time $t = 0$, we apply an oscillatory point force at the equator of the shell with $\omega \approx 1$ (left) or $\omega \approx 5$ (right). For $\omega \sim 1$ the analytic theory predicts a wide range of incident angles leading to TIR – see Figs. 3a,b, bottom panel; we see that for short times waves are confined to the saddle region reflected off the top and bottom boundaries – see Fig. 4a. Over time they leak into the spherical caps due primarily to transmission occurring at normal incidence, as expected from the theory – see Fig. 3b, bottom panel. For $\omega \approx 5$, the interface is predicted to be essentially transparent; indeed, the simulation shows that waves propagate propagate freely across the boundary – see Fig. 4b.

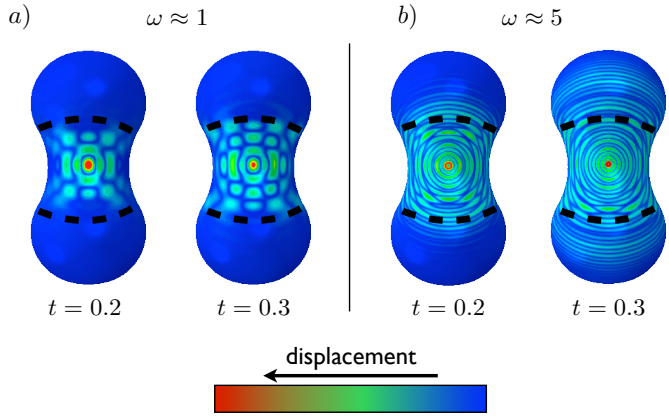

FIG. 4: (Color online) Finite element simulations showing total internal reflection at the boundary of negative and positive Gaussian curvatures, denoted by the dashed line. a) For $\omega \approx 1$, the linear theory predicts a range of incident angles for which rays exhibit TIR. For this shell, with $\beta \approx -0.5$, the rays propagate preferentially at $\theta^* \sim \tan^{-1}(\sqrt{-\beta}) \approx 35°$, which falls within the predicted band of incident angles for TIR. The shell does not have a constant curvature, and we use a point force instead of a plane wave so the wave trapping is temporary. Over longer times they leak into the positive Gaussian curvature region. b) For $\omega \approx 5$ the shell is predicted to be essentially transparent. This too is supported by the simulation.

We have shown the utility of an analogy to geometric optics for understanding the dynamics of flexural waves on surfaces of nontrivial geometry. Curvature acts as the local index of refraction and interfaces between positive and negative Gaussian curvature in particular lead to total internal reflection of waves propagating from the negative curvature side. This suggests that such boundaries generate causally disconnected regions on the manifold such that flexural waves in the two sectors cannot equilibrate, at least within our linear analysis. The implications for the statistical mechanics of such waves on manifolds of complex geometry have not been explored. More generally, one may inquire about the role of localization and enhanced backscattering from randomly curved surfaces even without the singular limit of crumpling [34–36]. In addition to such random shapes one may be able to use prescribed geometries to redirect flexural waves with a purely geometric wave-guide to "cloak" regions of the membrane, as has been explored using anisotropic metamaterials [37]. Nonlinearities ignored here are known, in some cases, to lead to anomalous elasticity [7, 27] and result in dynamical equations reminiscent of weak turbulence [38]; the role of geometry in such cases remains to be fully explored.

A.J.L. thanks L. Mahadevan for enjoyable conversations. The authors acknowledge Grant No. NSF DMR-1006162.

[1] C. Bower, R. Rosen, L. Jin, J. Han, and O. Zhou, Appl. Phys. Lett. **74**, 3317 (1999).

[2] P. Kearey, K. A. Klepeis, and F. J. Vine, *Global tectonics* (Wiley-Blackwell, 2009).

[3] J. Lidmar, L. Mirny, and D. R. Nelson, Phys. Rev. E **68**, 051910 (2003).

[4] T. Kuriabova and A. J. Levine, Phys. Rev. E **77**, 031921 (2008).

[5] Y. K. Park, C. A. Best, K. Badizadegan, R. R. Dasari, M. S. Feld, T. Kuriabova, M. L. Henle, A. J. Levine, and G. Popescu, Proc. Natl. Acad. Sci. USA **107**, 6731 (2010).

[6] Y. K. Park, C. A. Best, T. Kuriabova, M. L. Henle, M. S. Feld, A. J. Levine, and G. Popescu, Phys. Rev. E **83**, 051925 (2011).

[7] J. Paulose, G. A. Vliegenthart, G. Gompper, and D. R. Nelson, Proc. Natl. Acad. Sci. USA **109**, 19551 (2012).

[8] J. Dervaux and M. Ben Amar, Phys. Rev. Lett. **101**, 068101 (2008).

[9] C. Py, P. Reverdy, L. Doppler, J. Bico, B. Roman, and C. N. Baroud, Phys. Rev. Lett. **98**, 156103 (2007).

[10] J. Kim, J. A. Hanna, M. Byun, C. D. Santangelo, and R. C. Hayward, Science **335**, 1201 (2012).

[11] Y. Klein, E. Efrati, and E. Sharon, Science **315**, 1116 (2007).

[12] L. Pocivavsek, R. Dellsy, A. Kern, S. Johnson, B. Lin, K. Y. C. Lee, and E. Cerda, Science **320**, 912 (2008).

[13] B. Roman and J. Bico, J. Phys.: Condens. Matter **22**, 493101 (2010).

[14] A. A. Evans and E. Lauga, Phys. Rev. E **79**, 066116 (2009).

[15] H. King, R. D. Schroll, B. Davidovitch, and N. Menon, Proc. Natl. Acad. Sci. USA **109**, 9716 (2012).

[16] B. Davidovitch, R. D. Schroll, D. Vella, M. Adda-Bedia, and E. A. Cerda, Proc. Natl. Acad. Sci. USA **108**, 18227 (2011).

[17] A. Vaziri, Thin Wall. Struct. **47**, 692 (2009), ISSN 0263-8231.

[18] A. A. Evans, S. E. Spagnolie, D. Bartolo, and E. Lauga, Soft Matter **9**, 1711 (2013).

[19] D. Vella, A. Ajdari, A. Vaziri, and A. Boudaoud, Phys. Rev. Lett. **109**, 144302 (2012).

[20] A. Lazarus, H. C. B. Florijn, and P. M. Reis, Phys. Rev. Lett. **109**, 144301 (2012).

[21] A. Vaziri and L. Mahadevan, Proc. Natl. Acad. Sci. USA **105**, 7913 (2008).

[22] F. I. Niordson, *Shell Theory* (North-Holland, 1985).

[23] T. R. Powers, Rev. Mod. Phys. **82**, 1607 (2010).

[24] E. Cerda and L. Mahadevan, Proc. R. Soc. A **461**, 671 (2005).

[25] E. Cerda and L. Mahadevan, Phys. Rev. Lett. **80**, 2358 (1998).

[26] L. D. Landau and E. M. Lifshitz, *Theory of elasticity* (Pergamon Press, Oxford, 1986), 3rd ed.

[27] D. R. Nelson, *Defects and geometry in condensed matter physics* (Cambridge University Press, 2002).

[28] H. Goldstein, *Classical mechanics* (Addison-Wesley Pub. Co., 1980).

[29] O. A. Germogenova, J. Acoust. Soc. Am. **53**, 535 (1973).

[30] A. N. Norris, Wave Motion **21**, 127 (1995), ISSN 0165-2125.

[31] A. N. Norris and D. A. Rebinsky, J. Vib. Acoust. **116**, 457 (1994).

[32] A. A. Evans and A. J. Levine, to be published (2013).

[33] M. Born and E. Wolf, *Principles of optics: electromagnetic theory of propagation, interference and diffraction of light* (Cambridge university press, 1999).

[34] T. A. Witten, Rev. Mod. Phys. **79**, 643 (2007).

[35] A. Gopinathan, T. A. Witten, and S. C. Venkataramani, Phys. Rev. E **65**, 036613 (2002).

[36] G. Seizilles, E. Bayart, M. Adda-Bedia, and A. Boudaoud, Phys. Rev. E **84**, 065602 (2011).

[37] N. Stenger, M. Wilhelm, and M. Wegener, Phys. Rev. Lett. **108**, 014301 (2012).

[38] G. Düring, C. Josserand, and S. Rica, Phys. Rev. Lett. **97**, 025503 (2006).